Acta Pharmaceutica Sinica B 2021;11(1):283–299

Chinese Pharmaceutical Association
Institute of Materia Medica, Chinese Academy of Medical Sciences

Acta Pharmaceutica Sinica B

www.elsevier.com/locate/apsb
www.sciencedirect.com

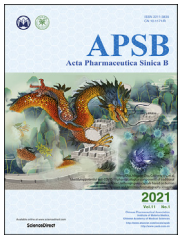

ORIGINAL ARTICLE

A pentapeptide enabled AL3810 liposome-based glioma-targeted therapy with immune opsonic effect attenuated

Jinyang Li[a], Jiasheng Lu[a], Haiyan Guo[a], Jianfen Zhou[a], Songli Wang[a], Kuan Jiang[a], Zhilan Chai[a], Shengyu Yao[a], Xiaoyi Wang[a], Linwei Lu[d], Cao Xie[a], Yi Chen[b], Weiyue Lu[a,c,d,e,*]

[a]*Department of Pharmaceutics, School of Pharmacy, Fudan University & Key Laboratory of Smart Drug Delivery (Fudan University), Ministry of Education and PLA, Shanghai 201203, China*
[b]*Chinese Academy of Sciences Shanghai Institute of Materia Medica, Shanghai 201203, China*
[c]*State Key Laboratory of Medical Neurobiology and MOE Frontiers Center for Brain Science, Institutes of Brain Science, Fudan University, Shanghai 200032, China*
[d]*The Institutes of Integrative Medicine of Fudan University, Shanghai 200041, China*
[e]*Minhang Branch, Zhongshan Hospital and Institute of Fudan-Minghang Academic Health System, Minghang Hospital, Fudan University, Shanghai 201199, China*

Received 7 April 2020; received in revised form 10 July 2020; accepted 15 July 2020

KEY WORDS

Liposome;
mn;
c(RGDyK);
Immune opsonization;
Immunogenicity;
Anti-glioma efficacy

Abstract AL3810, a molecular dual inhibitor of the vascular endothelial growth factor receptor (VEGFR) and fibroblast growth factor receptor (FGFR), has earned the permission of phase II clinical trial for tumor treatment by China FDA. As a reversible ATP-competitive inhibitor, AL3810 targets ATP-binding site on intracellular region of VEGFR and FGFR, whereas, AL3810 lacking interplay with extracellular region of receptors rendered deficient blood–brain tumor barrier (BBTB) recognition, poor brain penetration and unsatisfactory anti-glioma efficacy. Integrin $\alpha v\beta 3$ overexpressed on capillary endothelial cells of BBTB as well as glioma cells illuminated ligand-modified liposomes for pinpoint spatial delivery into glioma. The widely accepted peptide c(RGDyK)-modified liposome loading AL3810 of multiple dosing caused hypothermia, activated anti-c(RGDyK)-liposome IgG and IgM antibody and pertinent complements C3b and C5b-9, and experienced complement-dependent opsonization. We newly proposed a pentapeptide mn with superb $\alpha v\beta 3$-binding affinity and tailored AL3810-loaded mn-modified liposome that afforded impervious blood circulation, targeting ability, and glioma therapeutic expertise as vastly alleviated immune opsonization on the underpinning of the finite antibodies and complements

*Corresponding author. Tel.: +86 21 5198 0090.
E-mail address: wylu@shmu.edu.cn (Weiyue Lu).

Peer review under responsibility of Chinese Pharmaceutical Association and Institute of Materia Medica, Chinese Academy of Medical Sciences.

https://doi.org/10.1016/j.apsb.2020.07.024

assembly. Stemming from attenuated immunogenicity, peptide mn strengthened liposome functions as a promising nanocarrier platform for molecular targeting agents.

1. Introduction

Angiogenesis, the formation of new blood vessels from preexisting ones, is a hallmark of tissue repair, expansion, and remodeling in tumor pathologies to furnish the high proliferative rate of cancer cells involving the sprouting, migration and proliferation of endothelial cells. Angiogenesis is regulated by multiple factors among which vascular endothelial growth factor (VEGF) and fibroblast growth factor (FGF) play an instrumental role[1,2]. The improper development of tumor blood vessels is mediated by overexpressed VEGF and FGF receptor under guidance of VEGF and FGF secreted by tumor and stromal cells[3]. Moreover, there is a sound argument that many tumor types associated with high vascular density over-express VEGF, FGF and their receptors including glioma[4−6]. New compound 6-[[7-[(1-aminocyclopropyl) methoxy]-6-methoxy-4-quinolyl]oxy]-*N*-methyl-naphthalene-1-carboxamide, designated as AL3810, was synthesized to selectively block VEGF/VEGFR and FGF/FGFR axis for shutting off the reciprocal compensatory mechanisms[7]. As a tyrosine kinase inhibitors (TKIs) benefiting from highly selectivity and considerable potency, AL3810 did exceptional therapeutic management in a broad spectrum of human tumor xenografts. This compound also displayed minimal species differences and a better safety window compared with traditional chemotherapeutic agents, winning approval of phase II clinical trial by China Food and Drug Administration (CFDA) and Europe government[8].

Success in an intracranial glioma model has not been achieved, although AL3810 with an IC_{50} value of micromole concentrations in U87 MG cell line promises a practicable remedy technique for glioma. AL3810 is a reversible ATP-competitive inhibitor aiming at the ATP pocket on intracellular region of VEGFR and FGFR[8], but paucity in specific recognition with VEGFR- or FGFR-enriched blood−brain tumor barrier (BBTB) results from lacking interplay with extracellular recognition region of receptors. In addition, BBTB has less frequent transendothelial cell fenestrations and smaller inter-endothelial cell gaps than that of peripheral tumors microvasculature[9−12], which hinders AL3810 to reach a sufficient concentration in glioma front. Like other TKIs such as erlotinib, gefitinib, and lapatinib[13,14], AL3810 failed in glioma model due to poor brain penetration. This dilemma of curing central nervous system cancers lays stress on the existence of BBTB, and expedites burgeon of target-molecule-decorated nanomedicine for BBTB targeting and transcytosis[15−17].

Peptide c(RGDyK) is pervasively explored to decorate nanocarriers for glioma-targeted drug delivery based upon recognition specificity with integrin $\alpha v\beta 3$[11]. Integrin $\alpha v\beta 3$ overexpressed on the tumor neovasculature as well as glioblastoma cells is of key importance to tumor progression which has been regarded as an appealing target for glioblastoma therapy[18]. Ideally as c(RGDyK)-liposome loading chemotherapeutic agents treated glioma, our group found that c(RGDyK)-liposome encapsulating molecular targeting agents of repeated administration could induce an immune complex-driven acute systemic anaphylaxis with being routed into rapid elimination and dysfunction of spatial delivery to glioblastoma milieu[19,20]. We disclosed that c(RGDyK)-liposome was devastated by the fact-based immune opsonization as a vast collection of antibodies and complements production and binding. To consummate the $\alpha v\beta 3$-targeted liposome used for transporting AL3810 into glioma crossing BBTB, we devised a novel linear pentapeptide which was named as mn (Amino acid sequence: mnRwr, capital letter stands for L-amino acid; lower case letter stands for D-amino acid) with $\alpha v\beta 3$-binding affinity[21].

In this study, we substantiated the glioma-targeted capability of peptide mn and successfully tailored the AL3810-loaded liposome. With BBTB permeability of peptide-modified AL3810-loaded liposomes elucidated, we compared biosafety of c(RGDyK)-modified and mn-modified AL3810-loaded liposomes. We highlighted the problematic root of rapid clearance from the blood compartment and unveiled the adverse effect of immune opsonization that immunogenicity brought about. Using widely acceptable c(RGDyK)-modified liposome as an appropriate comparison, mn-strengthened liposome with attenuated immunogenicity surmounted the opsonic effect and extended the remedy benefit of AL3810 significantly, proclaiming a superior nanocarrier platform for molecular targeting agents.

2. Materials and methods

2.1. Materials

Peptide c(RGDyK) and mn were synthesized by KareBay Biochem, Inc. (Ningbo, China). Hydrogenated soy phosphatidylcholine (HSPC) and $mPEG_{2000}$-DSPE were supplied by Lipoid GmbH (Ludwigshafen, Germany). Mal-PEG_{3400}-DSPE was supplied by Laysan Bio Co. (Arab, USA). Cholesterol and 5-carboxyfluorescein (FAM) was bought from Sigma−Aldrich (St. Louis, MO, USA). DAPI and fluorescein-5-maleimide were from Fanbo Biochemicals (Beijing, China). Near infrared dye DiR (1,1′-dioctadecyl-3,3,3′,3′-tetramethyl indotricarbocyanine iodide), DiD (1,1′-dioctadecyl-3,3,3′,3′-tetramethyl indodicarbocyanine, 4-chlorobenzenesulfonate salt dye), LysoTracker®Red DND-99 and agarose gel were supplied by Invitrogen (Grand Island, NY, USA). TEM grids were purchased from Beijing XXBR Technology Co., Ltd., (Beijing, China). And mouse serum was from Shanghai YuanMu Biological Technology Co., Ltd., (Shanghai, China). Apoptosis Kit and MTT (thiazolyl blue tetrazolium bromide) were obtained from Dalian Meilun Biology Technology Co., Ltd., (Dalian, China). Growth factor reduced Matrigel matrix was obtained by BD Biosciences (San Diego, CA, USA). Peroxidase-Conjugated AffiniPure Goat Anti-Mouse IgG(H+L) was bought from ZSGB-BIO (Beijing, China). SDS-PAGE precast gel (Tris-Gly, 4%−20%, 12 well), SDS-PAGE 5× sample loading buffer, Fast Silver Stain Kit and 3,3′,5,5′-tetramethylbenzidine (TMB) were supplied by Beyotime Institute of Biotechnology (Shanghai, China). Goat anti-mouse IgM mu chain (HRP, ab97230), anti-CD31 antibody (ab28364), rabbit anti-

VEGF receptor 1 antibody (ab2350), rabbit anti-FGFR1 antibody (ab76464), goat anti-rabbit IgG H&L (Alexa Fluor® 488, ab150077) and rabbit anti-C3 antibody (ab200999) were purchased from Abcam (Cambridge, UK). Recombinant human FGF basic/FGF2/bFGF (146 aa) protein and recombinant human VEGF 165 protein were from R&D System (Minneapolis, MN, USA). Rat terminal complement complex C5b-9 ELISA kit and rat complement fragment 3b ELISA kit were supplied by Shanghai Enzyme-linked Biotechnology Co., Ltd., (Shanghai, China). Rabbit anti-CD35 antibody was bought from Beijing Bioss Antibodies Biotechnology Co., Ltd., (Beijing, China). All other reagents were from China National Pharmaceutical Group Corporation (Shanghai, China).

Human glioblastoma cells (U87 MG cells) was from American type culture collection (ATCC, Manassas, VA, USA), and Human umbilical vascular endothelial cells (HUVECs), Leukemia cells in mouse macrophage (RAW264.7 cells) and alpha mouse liver 12 cells (AML12 cells) were obtained from Shanghai Institute of Cell Biology (Shanghai, China). All cells were cultured in Dulbecco's modified Eagle's medium (Gibco) containing 10% FBS (Gemini), 100 μg/mL streptomycin (Gibco) and 100 U/mL penicillin (Gibco) at 37 °C in a humidified atmosphere containing 5% CO_2. Male BALB/c nude mice of 4−6 week age were supplied by Lingchang Biotech (Shanghai, China) and Sprague−Dawley (SD) rats around 120 g and ICR mice about 25 g were from the BK Lab Animal Ltd. (Shanghai, China) and all housed under SPF conditions. All animal protocols were agreed by the Ethics Committee of Fudan University, Shanghai, China.

2.2. Cellular targeting ability of peptide

Fluorescein-labeled peptides were synthesized by sulfhydryl-maleimide covalent conjugation. Fluorescein-5-maleimide in DMF (20 mg/mL) was added to peptide solution (5 mg/mL; solvent: PBS) dropwise with constant stirring. The crudes were purified by preparative C18 RP-HPLC, and the separations were analyzed by analytical RP-HPLC and ESI-MS to verify purity and structure. c(RGDyK)-FITC and mn-FITC were diluted into 5 μmol/L with DMEM containing 10% FBS, and then utilized to culture U87 MG cells and HUVECs in 37 °C for 4 h. Next, 50 nmol/L LysoTracker®Red was added to visualize lysosome. After 0.5 h, cells were rinsed, fixed with 4% formaldehyde and stained by 1 nmol/L DAPI. The intracellular fluorescence was captured by confocal microscope (Leica, Wetzlar, Germany). Three-dimensional tumor spheroids were also established to validate the tumor-penetrating ability. Agarose gel was diluted into 2% by DMEM and then through moist heat sterilization, which was added into a 48-well plate about 150 μL per well. Awaiting cooling down, U87 MG cells were plated onto gel at a density of 3×10^3/400 μL per well. Ageing for ten days roughly, the multicellular tumor spheroids with round shape were transferred into four-well chambered cover-glass with 500 μL DMEM (10% FBS) containing 5 μmol/L fluorescein-labeled peptide per well. FAM served as the negative control. The penetrating depth and intensity of fluorophore on tumor spheroids was observed using confocal microscopy (Leica, Wetzlar, Germany) with Z-stack imaging at ~5 μm intervals. Competitive inhibition experiment was conducted by blocking $\alpha v\beta 3$ integrin of U87 MG cells with excessive c(RGDyK) in 4 °C. U87 MG cells were incubated with 5 μmol/L various peptide fluoresceins for 4 h. Cells were trypsinized, washed and counted by flow cytometry (BD Biosciences).

2.3. In vivo targeting ability of peptide

U87 MG cells (5×10^6 cells in 100 μL PBS) were transplanted on male BALB/c nude mice subcutaneously to form xenograft tumor model. The subcutaneous U87 MG tumor-bearing mice 14 days post-implantation were injected with 200 μL 100 μmol/L different peptide fluoresceins and sacrificed after 4 h. Having been perfused, the tumors were harvested and processed into the frozen section, following staining with 300 nmol/L DAPI for 10 min. CD31 was characterized by anti-mouse CD31 antibodies and stained with Alexa 594-conjugated secondary antibodies to visualize tumor angiogenesis. The sections were inspected by confocal microscope.

2.4. Preparation of liposome

Liposomes were prepared by thin-film hydration and ultrasound method[20]. To prepare blank liposomes (without loading of payload), the formulation of plain liposome (LS, without targeting ligand), liposome with c(RGDyK) modification [c(RGDyK)-LS] and liposome with mn modification (mn-LS) as follows: HSPC/cholesterol/$mPEG_{2000}$-DSPE (molar ratio, 50:45:5) or HSPC/cholesterol/$mPEG_{2000}$-DSPE/c(RGDyK)-PEG_{3400}-DSPE (molar ratio, 50:45:3:2) or HSPC/cholesterol/$mPEG_{2000}$-DSPE/mn-PEG_{3400}-DSPE (molar ratio, 50:45:3:2). The sulfhydryl-maleimide coupling method was adopted to synthesize mn-PEG_{3400}-DSPE and c(RGDyK)-PEG_{3400}-DSPE by using thiolated peptides and Mal-PEG_{3400}-DSPE. All excipients were dissolved in chloroform completely and then rotary evaporated to form a thin film, following drying overnight under vacuum. With normal saline added, the film was hydrated at 60 °C for 1 h before the resultant crude emulsion was homogenized by probe ultrasound and eventually filtered by mixed cellulose ester millipore. Liposomes encapsulating DiD or DiR was fulfilled *via* the same procedure except that DiD or DiR was incorporated into thin-film formation. The nanoparticle size distribution of different liposomes was evaluated by dynamic light scattering (DLS) method (Malvern zeta sizer 3000, Malvern, Worcestershire, UK). The concentration of DiD and DiR were calculated by fluorescence spectrophotometer (Cary Eclipse, Agilent, Santa Clara, CA, USA) at E_x/E_m 625/660 and 741/776 nm, respectively.

Plain AL3810-loaded liposome (LS/AL3810, without targeting ligand), AL3810-loaded liposome with c(RGDyK) modification (c(RGDyK)-LS/AL3810) and AL3810-loaded liposome with mn modification (mn-LS/AL3810) were formulated by ammonium sulfate gradient loading method at a molar ratio of 4.65 (excipients: drug). Liposomes loading ammonium sulfate were prepared as aforementioned other than ammonium sulfate hydration alternatively, and through gel filtration over a Sephadex G-50 column against normal saline. The mixture between liposome and AL3810 citric acid solution was directly added with 1 mol/L Na_2HPO_4 for pH adjustment to 5.7 prior to incubation at 60 °C for 0.5 h. The successful preparation of liposomes encapsulating AL3810 were realized by removing unloaded AL3810 by Sephadex G-50 column (Sigma−Aldrich, St. Louis, MO, USA). AL3810 solution

(25 μg/mL) was scanned within 200−600 nm wavelength by ultraviolet spectrophotometer (Shimadzu, Kyoto, Japan) to ascertain the appropriate wavelength. Ultimately AL3810 loading efficiency was measured by RP-HPLC, conditions of which were listed as follows: (1) Agilent 1260 series (Santa Clara, CA, USA). (2) C18 column (YMC, Kyoto, Japan). (3) UV detection wavelength 239 nm. (4) mobile phase A: 10 mmol/L ammonium acetate, mobile phase B: acetonitrile. (5) gradient elution: 0−20 min 20% B−95% B. (6) flow rate: 0.7 mL/min. (7) injection volume: 20 μL.

2.5. Characterization of liposome

To confirm the morphology, we performed High-Resolution Transmission Electron Microscope (TECNAIS-TWIN, Portland, OR, USA) characterization. TEM grids were immersed with five-times-diluted liposome for 5 min and dried in bake oven. After that, grids were negatively dyed against phosphotungstic acid and aired overnight. Next, we observed stabilities of liposomes in PBS and 50% mouse serum, and recorded the changes of size and PDI that were gauged by Malvern Zeta sizer 3000. Dialysis bag (MWCO 14 kDa) was employed to simulate *in vitro* leakage kinetics of AL3810 from AL3810-loaded liposomes. For leakage study in PBS, inner phase and external phase were 1 mL liposomes containing 1 mg AL3810 and 20 mL PBS (0.5% Tween 80, *v*/*v* 1:200), respectively; for leakage study in serum, counterparts were 0.3 mL mouse serum with 0.7 mL liposomes containing 0.5 mg AL3810 and 6 mL mouse serum with 14 mL PBS, respectively. At predesigned time points, 0.5 mL external aqueous phase was sampled, after-processed for protein sedimentation and quantified by RP-HPLC.

2.6. Hemolysis safety of AL3810 formulations for intravenous injection

2 mL fresh mouse blood was washed by 20 mL normal saline gently, and afterwards, centrifuged at 1500 rpm (Xiangyi, Changsha, China) for 15 min to eradicate the supernatant. Then the precipitated red blood cells were washed by normal saline for 2−3 times until the supernatant did not manifest any red. Finally, red blood cell suspension (*v*:*v*, 1:50) was compounded by dilution with normal saline, which was subsequently incubated with the same volume of 700 μg/mL AL3810 formulations at 37 °C for 2 h. Free drug AL3810 was dissolved in a mixture of PBS, Tween 80 and ethanol (*v*:*v*:*v*, 90:5:5). The hemolysis was photographed after centrifugation at 3000 rpm (Xiangyi) for 10 min and 500 μL supernatant was measured by ultraviolet spectrophotometer at 540 nm. Distilled water was employed as positive control and PBS as negative control. Hemolysis ratio was calculated based on the following Eq. (1):

$$\text{Hemolysis ratio}(\%) = \left(A_{\text{Sample}} - A_{\text{Negative}}\right) / \left(A_{\text{Positive}} - A_{\text{Negative}}\right) \times 100 \quad (1)$$

2.7. In vivo targeting ability of peptide-modified liposome

The glioma orthotopic xenograft was constructed as reported previously[22]. The glioma orthotopic xenograft-bearing mice 14 days post-implantation were randomly grouped ($n = 3$) and administrated with various DiR-loaded liposomes at the DiR dose of 300 μg/kg (DiR to bodyweight). A time-course experiment (1, 2, 4, 8, 12 and 24 h) for *in vivo* tracking fluorophore was carried out and semi-quantitative ROI was also analyzed.

2.8. Cellular effect of peptide-modified AL3810-loaded liposome

U87 MG cells and HUVECs were seeded onto 12-well plates at a density of 10^5 cells and 3×10^5 cells per well overnight, which were substituted by various treatments of equal AL3810 concentration (180 μg/mL) the next day. Cells were trypsinized, rinsed, counted by Automated Cell Counter (Countstar, Shanghai, China) and ultrasonicated after 4-h drug exposure, following re-suspending in acetonitrile. Supernatant was procured by centrifugation at 12,000 rpm (Thermo fisher, Waltham, MA, USA) for 20 min and then quantified by C18 RP-HPLC. Study on glioma cells apoptosis induction was on the basis of co-incubation with multiple remedies for 24 h at the same AL3810 concentration (15 μmol/L). Cells were trypsinized, rinsed and stained with Annexin V-FITC and PI by manufacture instruction preceding count by flow cytometry. To test the regulation AL3810 remedies exerted on VEGFR on glioma cells, pre-plated U87 MG cells were incubated with various 20 μmol/L AL3810 formulations for 24 h. When reaching the time point, cells were rinsed, trypsinized and stained with 1% bovine serum albumin (BSA), rabbit anti-VEGF receptor 1 antibody, goat anti-rabbit IgG H&L (Alexa Fluor® 488) by turn. Cellular fluorescence intensity was quantified by flow cytometry. MTT assay was conducted to appraise cytotoxicity likewise. U87 MG cells that were seeded onto 96-well plates at a density of 3000 cells per well the day before, were incubated with AL3810 formulations in a series of concentration for 4 and 72 h. Subsequently cells were exposed to MTT (5 mg/mL, 20 μL per well) for 4 h, surveyed by Microplate Reader (Bio Tek, Winooski, VT, USA). IC_{50} was generated by fitting the data with nonlinear regression using GraphPad Prism 7 (GraphPad Software, San Diego, CA, USA). To substantiate the anti-angiogenesis effect of AL3810 against VEGF and FGF stimulation, the pre-seeded HUVECs were exposed to different AL3810 treatments for 2 h and subjected to 50 ng/mL VEGF165 or 25 ng/mL b-FGF for 72 h. MTT detection was performed as described above. Matrigel basement was used to model tumoral neovascularization by pre-coating onto 24-well plates. Trypsinized HUVECs suspended in 30 μmol/L AL3810-encompassing DMEM medium were mixed with 50 ng/mL VEGF165 or 25 ng/mL b-FGF, which were seeded on Matrigel overnight. The tube structure destructiveness was observed by an inverted phase contrast microscope (DMI4000B, Leica). A drug-free DMEM aliquot was subject to the same procedure as control. The amount of tubes was calculated within three randomly selected vision fields.

2.9. Intracranial distribution of peptide-modified AL3810-loaded liposome

At 14 days post inoculation, the randomly sorted groups ($n = 3$) were injected with free drug, LS/AL3810, c(RGDyK)-LS/AL3810 and mn-LS/AL3810, respectively *via* tail vein at one single dose of 2 mg/kg (AL3810 to bodyweight). The right hemisphere of brain where U87 MG cells were planted was harvested, weighed and homogenized followed by execution and perfusion at 4 h after injection. 200 μL homogenate was mixed with 100 μL methanol, vortexed for 2 min. After being centrifuged at 12,000×*g* for 10 min, 80 μL supernatant was put into HPLC measurement. A

concentration gradient of AL3810 was exploited for fitting calibration curves.

2.10. Safety and immunogenicity evaluation on ICR mice

Male ICR mice were assigned into 5 groups ($n = 3$) and administrated with LS/AL3810, c(RGDyK)-LS/AL3810, mn-LS/AL3810 and saline, respectively *via* tail vein at dose of 4 mg AL3810/kg/administration on Days 0, 2, 4, 6 and 8. The temperature of mice was measured with infrared forehead thermometer (MC-872 K, OMRON, Kyoto, Japan, measurement range: 0−50 °C) at 30 min post completing each administration. For anti-liposome IgG and IgM qualification *via* ELISA analysis, blood was sampled from the retro-orbital sinus on Days 7, 10 and 14. ELISA protocol was as follows. Antigen (various liposomes) was diluted by ethanol and coated into 96-well plates overnight, washed by 0.05% Tween/PBS. After being blocked by 150 μL PBS with 1% BSA, the coated wells were filled with serial dilutions of serum (diluent solvent was PBS) and incubated at 37 °C for 1 h. Concisely, IgG binding onto plates was marked by Peroxidase-Conjugated AffiniPure Goat Anti-Mouse IgG(H+L), and IgM binding onto plates was marked by Peroxidase-Conjugated Goat Anti-Mouse IgM mu chain. The enzyme substrate solution (TMB) was added for initializing the enzyme reaction and 2 mol/L sulphuric acid for termination. Ultra violet absorbance at 450 nm was measured by Microplate Reader (Bio Tek, Winooski, VT, USA) as an indication of antibody titer in blood.

2.11. Comprehensive assessment of multiple dosing on SD rats

twb 0.22wThe grouped male SD rats were administrated with drug-free liposomes (LS, c(RGDyK)-LS, mn-LS and saline, respectively) *via* tail vein on Days 0 and 3 (dose: 52.5 μmol HSPC/kg/administration). On Day 6, rats were administrated with drug-loaded liposomes (LS/AL3810, c(RGDyK)-LS/AL3810, mn-LS/AL3810 and AL3810, respectively) *via* tail vein at AL3810 dose of 5 mg/kg. 500 μL blood was sampled from the retro-orbital sinus at indicated time points once starting injection. Of note, blood collected before administration was tagged as “0 h”. For pharmacokinetics profile, 200 μL plasma were separated after the centrifugal step at 4000 rpm (Xiangyi) for 10 min, which was subsequently admixed with 800 μL methanol and vortexed for 2 min. 80 μL supernatant drug inclusion was attained by centrifugation at 6000 rpm (Xiangyi) for 10 min and detected by RP-HPLC. Mixtures of blank plasma with concentration gradient of AL3810 were exploited for fitting calibration curves. To eradicate the antibody−liposome complex, the supernatant fraction of free antibody was separated by ultracentrifugation at 14,000×*g* for 30 min in 4 °C[23]. For free anti-liposome IgG and IgM antibody concentration tracking, the ultra-centrifuged plasma of 0, 0.5, 4 and 72 h were tested *via* ELISA assay as aforesaid. Corresponding liposome served as antigen. Determination of free C5b-9 and C3b concentration changes was performed by using ELISA kits following manufacture instruction. Reference standards were used for fitting calibration curves.

To characterize interplay of antibody and liposome *in vitro*, the plasma collected at 0 h or blank plasma was incubated with the same volume of corresponding liposome (the equal amount of phospholipid) by using Eppendorf Protein LoBind Tube in 37 °C for 1 h. The tubes were photographed for record. The pellet was procured by centrifugation at 14,000×*g* in 4 °C, and rinsed with cold PBS twice. The ultimate pellet was reconstituted by 60 μL PBS and added 15 μL SDS-PAGE 5× sample loading buffer following boiling at 100 °C for 10 min. Electrophoresis was performed using gradient polyacrylamide gel where 5 μL sample was loaded and 2 μL plasma was loaded as control. One should be noted that the tube of c(RGDyK)-LS/AL3810 with plasma sampled from c(RGDyK)-LS/AL3810 injected SD rat at 0 h was merely taken 0.5 μL for loading on account of the protein absorbate thickness. The gel was pictured after being stained with Fast Silver Stain Kit. The band 1−3 was analyzed by nano-LC−MS/MS on an LTQ Orbitrap Fusion mass spectrometer (Thermo Electron, San Jose, USA) as the previously documented method[23]. For cellular uptake trial after plasma binding, near-infrared fluorescent DiD-loaded liposomes were tailored and mixed with the corresponding plasma collected at 0 h alike. After incubation in 37 °C for 1 h, the tubes were photographed. U87 MG cells seeding on four-well chambered cover-glass were exposed to mixture dilution (equal DiD concentration of 200 nmol/L) in 37 °C for 4 h. Cells were rinsed, fixed and stained with DAPI, the intracellular fluorescence of which was observed by confocal microscope.

2.12. Immunized opsonization of liposomes by macrophage

Different DiD-loaded liposomes were incubated with the corresponding immune-activated plasma at a volume ratio of 9:1 aging in 37 °C for 1 h. The resultant opsonized liposomes diluted into DiD dosage of 500 nmol/L by DMEM culture were added to pre-seeded RAW264.7 cells for incubation in 37 °C for 4 h. Pristine liposomes were also conducted likewise for cellular uptake measuring. Cellular uptake by AML12 cells was operated as described above. AL3810-loaded liposomes and DOX-loaded liposomes in a row of concentrations were incubated with RAW264.7 cells for 48 h. MTT assay was performed as aforesaid. For colocalization of CD35 and opsonized DiD-labeled liposome, RAW264.7 cells were exposed to various opsonized liposome at a DiD dose of 500 nmol/L for 1 or 4 h. Subsequently, cells were rinsed and incubated with 1% BSA for blocking nonspecific adsorption preceding to incubation with 100 times diluted rabbit anti-CD35 antibody for 1h and 500 times diluted goat anti-rabbit IgG H&L (Alexa Fluor® 488) for 1 h.

2.13. Therapy efficiency on glioma orthotopic xenograft

After intracranial U87 MG glioma implantation on Day 0, the randomly assigned nude mice ($n = 10$) were injected with AL3810, LS/AL3810, c(RGDyK)-LS/AL3810 and mn-LS/AL3810 and saline, respectively *via* tail vein on Days 8, 10, 12, 14, 16, 18 and 20 with total AL3810 dose of 28 mg/kg (AL3810 to bodyweight). Survival time of mice and the body weight were recorded, and Kaplan−Meier survival curves were plotted for each group. The next day accomplishing treatments, CD31 immunohistochemical stain was to appraise glioma neovasculature. The excised brains were fixed with 4.0% paraformaldehyde, paraffin-embedded, sectioned and stained by anti-CD31 antibody. On the other hand, three immunofluorescent sections were obtained from each paraffin block: one for VEGFR, one for FGFR and one for TUNEL assay. The number

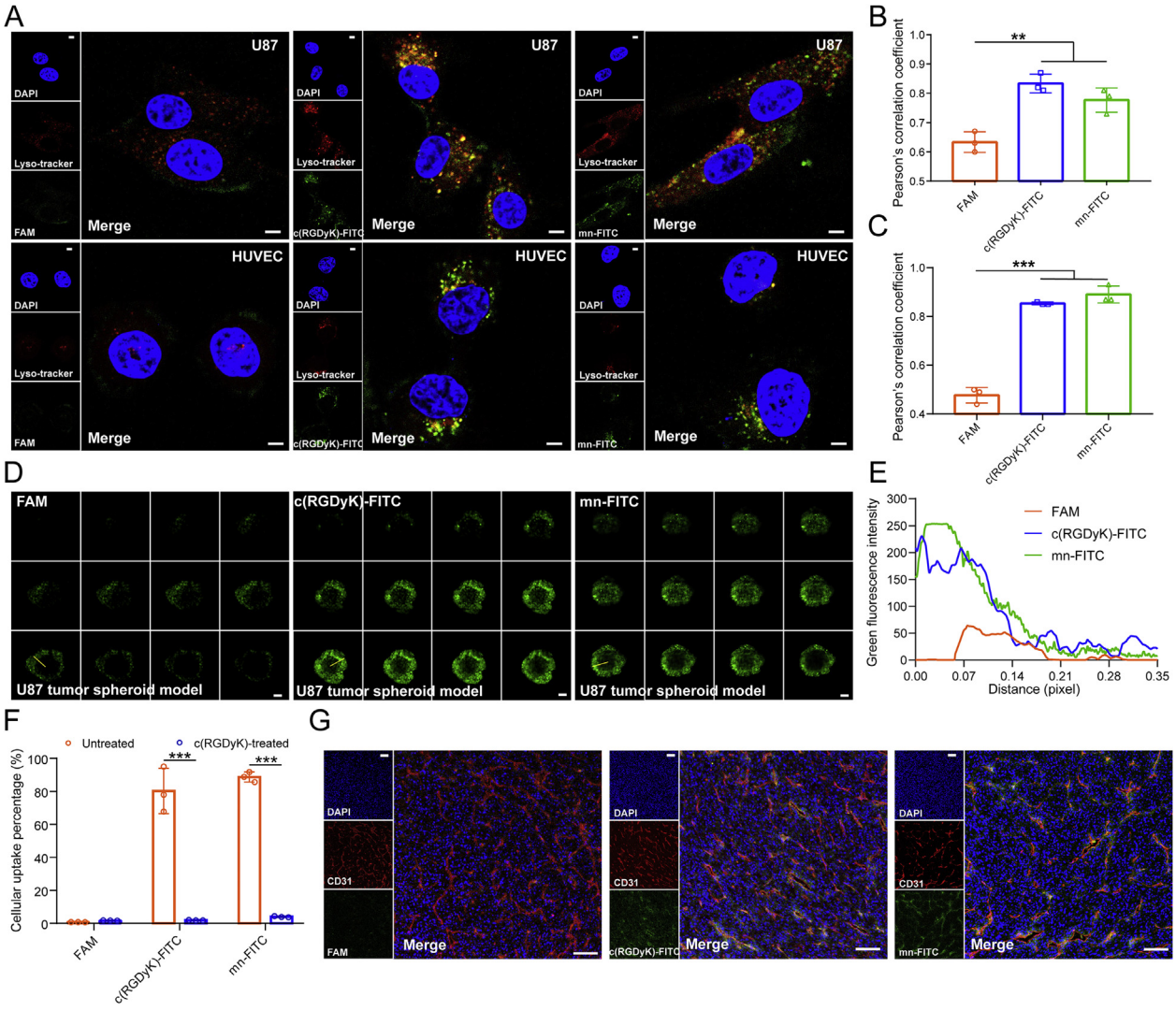

Figure 1 Targeting ability of peptide molecules. (A)−(C) The uptake of fluorescein-labeled peptides by U87 MG cells and HUVECs which were characterized by Lyso-tracker for endocytosis study. Intracellular fluorescence was captured by a confocal laser scanning microscope (A). Scale bar = 5 μm. Pearson's correlation coefficient between green fluorescence of peptide-FITC and red fluorescence of Lyso-tracker on U87 MG cells (B) and HUVECs (C) calculated by Image J software (Bethesda, USA) (Mean ± SD, $n = 3$, $^{**}P < 0.01$, $^{***}P < 0.001$). (D)−(E) The permeability of fluorescein-labeled peptides in *ex-vivo* U87 tumor spheroid model. The vertical depth of tumor spheroids was captured by confocal microscope with a 5 μm interval between consecutive slides (D). Scale bar = 200 μm. The green fluorescence of peptide-FITC calculated by pixel intensity along with distance from the periphery using Image J software (E). (F) Blocking experiment of fluorescein-labeled peptides on U87 MG cells by pre-incubation with c(RGDyK). Intracellular fluorescence was quantified by flow cytometry (Mean ± SD, $n = 3$, $^{***}P < 0.001$). (G) The intratumoral distribution of fluorescein-labeled peptides in subcutaneous U87 MG xenograft. Anti-CD31 antibody stained tumor angiogenesis and DAPI stained all cell nuclei. Scale bar = 100 μm.

of fluorescence-positive cells in glioma was counted. Hematoxylin-eosin staining sections of organs were cut to evaluate drug toxicity. And immunohistochemical analysis of immune complex depositions was also conducted to appraise immunological reaction in organs. Slides for analyzing immune complex deposition in liver and spleen were conducted as reported[20]. Rabbit anti-mouse C3 antibody at a dilution of 1:2000 was used for analyzing complement C3 deposition in liver.

2.14. *Statistical analysis*

Data were plotted as mean ± SD unless otherwise indicated. Comparison among the different groups was measured by the one-way ANOVA analysis. $P < 0.05$ was considered statistically significant.

3. Results and discussion

3.1. *Peptide mn had glioma recognition specificity via integrin αvβ3*

Fluorescein-labeled peptide mnRwrc-FITC (capital letter stands for L-amino acid; lower case letter stands for D-amino acid, referring to as mn-FITC in the following) and c(RGDyK)-FITC was successfully synthesized *via* sulfhydryl-maleimide covalent conjugation. The purity and structure were ascertained by

analytical C18 RP-HPLC and ESI-MS as shown in Supporting Information Fig. S1A−S1D. The conclusion that U87 MG cells and HUVECs ingested c(RGDyK)-FITC and mn-FITC avidly revealing significant difference from FAM was based on the captured intracellular green fluorescence distributed wholly throughout cytoplasm after peptide-fluorescein incubation (Fig. 1A). The impeccable colocalization with red-fluorescently labeled lysosome resulted in high Pearson's correlation coefficient, proffering a conjecture that lysosome might engage in the endocytic pathway of c(RGDyK)-FITC and mn-FITC (Fig. 1B and C). Taken together, mn-FITC and c(RGDyK)-FITC could be engulfed by U87 MG cells and HUVECs specifically, and disposed in lysosome. Thereafter, we trialed whether the endocytic pathway was largely contingent on $\alpha v\beta 3$-recognition by carrying out blockade experiment. $\alpha v\beta 3$ integrin was saturated after pre-incubation with excessive ligand c(RGDyK) in 4 °C, mn-FITC and c(RGDyK)-FITC were barely ingested demonstrating that internalization of mn-FITC was initialized by recognizing and anchoring $\alpha v\beta 3$ on the surface of cells (Fig. 1F). Tumor-penetrating ability of the glioma-targeted peptides was assessed through a three-dimensional tumor spheroid model established by U87 MG cells, which constituted the most common used *in vitro* model that recapitulated *in vivo* tumor microenvironment. FAM merely presented sporadic fluorescent puncta on the periphery of spheroid, but mn-FITC penetrated into tumor spheroid more deeply and intensely placed on a par with c(RGDyK)-FITC (Fig. 1D and E). Next then, *in vivo* tumor-targeted ability of mn-FITC was proved by massive accumulation in tumor tissue and considerable colocalization amount of tumor neovasculature visualized by anti-CD31 antibody (Fig. 1G), while c(RGDyK)-FITC retained moderately and FAM did not retain in tumor, that is to say, mn-FITC displayed slight superiority to c(RGDyK)-FITC in passage into tumor.

3.2. *mn-tethered liposome traversed into glioma*

The glioma orthotopic xenograft-bearing mice were injected with near infrared fluorescence-labeled liposomes for intracranial tracing. From the photograph of Supporting Information Fig. S2, mn-LS/DiR concentrated in brain marginally more than c(RGDyK)-LS/DiR did, which was in sharp contrast to LS/DiR. The results of semi-quantitative ROI analysis by the software (PerkinElmer, Waltham, MA, USA) of living image indicated that ligand-modified liposome could sufficiently enter brain soon and reach a spike in intracranial concentration about 2−4 h post administration. Integrin $\alpha v\beta 3$ was overexpressed on BBTB, offering an explanation why peptide mn facilitated receptor-mediated transcytosis of nanocarriers across BBTB in glioma.

3.3. *Drug AL3810 was successfully loaded into liposome*

AL3810 was a weakly alkaline and lipophilic small molecule agent. Quantitative analysis of AL3810 was implemented by using C18 RP-HPLC with UV detection (Supporting Information Fig. S1E and S1F). Firstly, we adopted the passive encapsulation method to load drug in hydrophobic phospholipid bilayer that turned out a low entrapment efficiency of 69.2%. AL3810 solubility surged enormously in acid circumstance to form strong acid-weak base salt, shedding a light on the likelihood of ammonium sulfate gradient loading method. The success loading counted on pH adjustment of AL3810 solution to 5.7 where most of AL3810 presented neutral molecule type that could pierce through phospholipid layer and did not precipitate (Supporting Information Fig. S3). Following this strategy, liposomes loaded with AL3810 displayed the same high encapsulation efficiency above 90% regardless of ligand modification or not (Supporting Information Table S1). The vesicle size of LS/AL3810 was distributed near 100 nm and peptide-modified AL3810-liposmes were about 110 nm because of thickened hydration layer formed by peptide-PEG_{3400}-DSPE, nevertheless, PDI (polydispersity index) was uniformly under 0.2 (Table S1 and Supporting Information Fig. S4A). Numerous round shapes of 80−100 nm in diameter and a modicum of multilamellar vesicles were observed under TEM (Fig. 2A). For stability assay, size of all AL3810-loaded liposomes stayed constant in PBS and 30% serum till 60 h showing the recalcitrant stability (Supporting Information Fig. S4B−S4E). Although PDI had a rather higher variance than size, PDI of all groups kept fluctuation under 120% till 60 h. Compared with free drug, each of the AL3810 liposomes represented sustained-release effect in PBS or serum (Supporting Information Fig. S4F and S4G). Concretely free drug leaked completely in 4 h but liposome leaked 20% in PBS and 40% in serum ultimately. The reason why the liposome leak kinetics in serum was notably slower than that in PBS (0.5% Tween 80) might be concerned with the precipitation of released drug in dialysis bag resulting from the poor solubility in serum. The leakage test could not mirror the genuine release fate *in vivo*, but evaluate stability and completeness of liposomes. Moreover, AL3810-loaded liposomes were not hemolytic speaking volumes about safety of excipients (Supporting Information Fig. S4H and S4I). The menstruum component Tween 80 of free drug formulation highly risked in hemolysis. To sum up, we succeeded in loading AL3810 into liposomes by active encapsulation method and clinching uniformity, stability and hemolytic safety of the formulated ligand-tethered liposomes.

3.4. *mn-LS/AL3810 had glioma-targeted preference*

We orchestrated assays to clarify whether ligand-modified AL3810-loaded liposomes could ship AL3810 to glioma *in vitro* and *in vivo*. As shown in Fig. 2B and C, U87 MG cells engulfed c(RGDyK)-LS/AL3810 and mn-LS/AL3810 more strongly than LS/AL3810 at disparity of 3.8- and 3.0-fold, respectively ($P < 0.001$); the counterpart for HUVECs was 1.3-fold equally ($P < 0.001$), manifesting the merit of receptor-mediated active transcytosis. Drug AL3810 was extracted from the right hemisphere of AL3810 formulation-injected nude mice bearing glioma orthotopic xenograft to compare the capability of crossing BBTB. Unambiguously, drug concentrations of AL3810 and LS/AL3810 group was simply 18.79% and 34.85% that of mn-LS/AL3810 group, respectively [Data for c(RGDyK)-LS/AL3810 group was 22.5% and 41.72%, respectively, Supporting Information Fig. S5]. Free drug AL3810 had a short blood duration (proved hereafter) so that traversing through BBTB was not adequate. Plain AL3810-loaded liposome had no affinity towards BBTB, which conduced to the limited intracranial drug amount. The BBTB-crossing profile of c(RGDyK)-LS/AL3810 and mn-LS/AL3810 was unraveled by proclivity to neovascularization and glioma

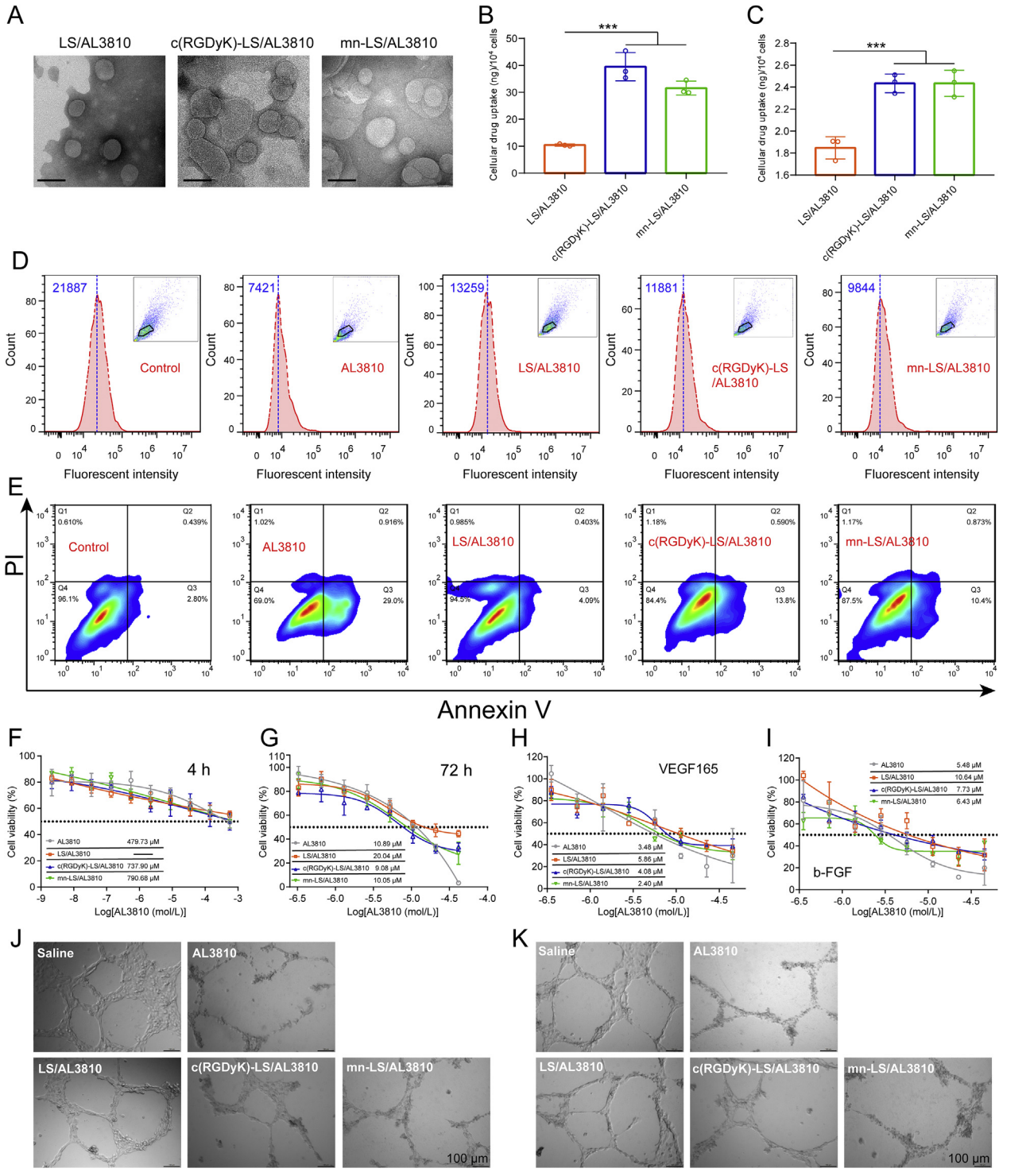

Figure 2 *In vitro* activity of the targeted AL3810-loaded liposomes. (A) TEM morphology characterization of various AL3810-loaded liposomes. Scale bar = 100 nm. (B) and (C) Cellular uptake of AL3810-loaded liposomes by U87 MG cells (B) and HUVECs (C). Quantification of drug concentration was conducted by RP-HPLC (Mean ± SD, $n = 3$, $^{***}P < 0.001$). (D) Expression level of VEGFR on U87 MG cells after various treatment. Anti-VEGFR antibody was used to recognize VEGFR and Alexa 488-conjugated second antibodies to facilitate fluorescence quantitation by flow cytometry. Median fluorescence was noted. (E) Apoptosis analysis of U87 MG cells treated with AL3810 and different AL3810 liposomes for 24 h. (F) and (G) Cytotoxic effect of AL3810 and different AL3810 liposomes on U87 MG cells through 4-h (F) and 72-h (G) incubation of drug containing medium. (H) and (I) Cytotoxic effect of AL3810 and different AL3810 liposomes on HUVECs stimulated by VEGF165 (H) and b-FGF (I). Cell viability was measured by MTT assay. Results were reflective of three replicates. (J) and (K) Destruction of different AL3810 loaded liposomes on neovascularization formed by HUVECs with VEGF165 (J) and b-FGF (K) stimuli. Scale bar = 100 μm.

parenchyma *via* αvβ3-mediated transcytosis from cytoplasm to distal cell membrane[24].

3.5. mn-LS/AL3810 had cytotoxicity on glioma and neovascularization

AL3810, a dual inhibitor of the VEGF and FGF receptors, inhibited VEGFR-1, -2, and -3, FGFR-1 and -2 kinases selectively and potently. VEGF/VEGFR and FGF/FGFR signaling of glioma were pervasively documented before[4–6], consequently a number of VEGF/VEGFR and FGF/FGFR-targeting agents have been trialed for glioma treatment. AL3810 could block VEGFR and FGFR, contributing to down regulation of receptor expression[25]. U87 MG cells incubated with AL3810 formulations decreased VEGFR expression to varying degrees. In detail, VEGFR expression were reduced by free drug AL3810 most evidently on account of transient passive diffusion into cytoplasm (Fig. 2D). Compared with LS/AL3810, mn-LS/AL3810 also hampered VEGFR expression like c(RGDyK)-LS/AL3810 demonstrating glioma cell preference of peptide-tethered liposomes. AL3810 killing glioma cell was induced by the initial interference with VEGF/VEGFR and FGF/FGFR signaling and finally underwent programmed cell death (so-called apoptosis). 29.0% U87 MG cells incubated with free drug AL3810 for 24 h stepped into early apoptosis counterpointing against 2.8% early apoptotic cells in untreated group, indicating the anti-proliferation effect on glioma cells (Fig. 2E). mn-LS/AL3810 and c(RGDyK)-LS/AL3810 elicited 10.4% and 13.8% early apoptosis, respectively benefiting from glioma tropism of liposomes endowed by peptide ligands. Apoptosis unfolded a route of AL3810 causing cell death reasoned from inhibition of ligand-dependent phosphorylation of VEGFR and FGFR signaling cascade. To calculate the half inhibitory concentration (IC_{50}), viabilities of U87 MG cells with AL3810 formulations exposure for 4 and 72 h were measured by MTT assay (Fig. 2F and G). The highest IC_{50} values for LS/AL3810 were in agreement with the least cellular uptake. The IC_{50} values for free drug AL3810, c(RGDyK)-LS/AL3810 and mn-LS/AL3810 in 4 h were 479.73, 737.90 and 790.68 μmol/L, which suggested the hallmark of that free drug directly contacted and worked fast to cells; the Data in 72 h were 10.89, 9.08 and 10.05 μmol/L, respectively, displaying the similar efficiency in anti-proliferation, and served as an ample evidence that the targeting liposomes could be internalized and release drug in intracellular milieu thoroughly. We found an inviable overall trend of the IC_{50} values toward HUVECs with VEGF165 and b-FGF stimulus (Fig. 2H and I). IC_{50} of AL3810, LS/AL3810, c(RGDyK)-LS/AL3810 and mn-LS/AL3810 against VEGF165 stimuli oriented at 3.48, 5.86, 4.08 and 2.40 μmol/L, respectively (Data against b-FGF stimuli was 5.48, 10.64, 7.73 and 6.43 μmol/L, respectively), which could be interpreted with effective suppression of ligand-dependent phosphorylation of VEGFR and FGFR on tumor angiogenesis. Furthermore, AL3810 did substantial catastrophic performance in neovascularization with inhibition rate over 97% whether VEGF165 or b-FGF stimuli (Fig. 2J and K and Supporting Information Fig. S6). c(RGDyK)-LS/AL3810 and mn-LS/AL3810 halted the 83% and 93% extensive and enclosed networks formation with VEGF165 or b-FGF stimuli equally, having significant difference from LS/AL3810 group that marginally restrained the tube formation. These results above corroborated that mn-LS/AL3810 had cytotoxicity on glioma cells and tumor neovascularization on the principle of inhibition of VEGF/VEGFR and FGF/FGFR axis.

3.6. c(RGDyK)-LS/AL3810 led to hypothermia

The male normal ICR mice were injected with various AL3810-loaded liposomes every second day for five times to simulate a remedy course, and the physical condition was surveyed after receiving treatments. We discovered the abnormality at 30 min post the fourth administration with the main symptom of a sudden drop in body temperature that only occurred to c(RGDyK)-LS/AL3810 group throughout the whole course (Supporting Information Fig. S7A). The hypothermia was hypersensitivity-like reaction drawing postulation to correlation with the aroused immune reaction[26], and therefore the blood was sampled for anti-liposome antibody evaluation (Supporting Information Fig. S7B and S7C). c(RGDyK)-LS/AL3810 bolstered immune system most fiercely with the robust production of anti-c(RGDyK)-liposome IgG and IgM antibody, unveiling a sustainable growth on Days 7−10 and peak on Day 10. Immune reaction was mildly provoked by mn-LS/AL3810 assumed as the slightly elevated IgG titer and comparable IgM titer with LS/AL3810. On Day 7, IgG and IgM antibody titer of c(RGDyK)-LS/AL3810 and mn-LS/AL3810 roughly perpetuated at the same level, but the latent immunogenicity of c(RGDyK)-motif was gradually ignited by multiple dosing. Safety profile of mn-LS/AL3810 was supported by low immunogenicity foreshadowing the promising application of AL3810 delivery into glioma.

3.7. Immunogenicity governed liposome clearance and targeting capability

As shown in Fig. 3A, SD rats with intact immune system were chosen for blood concentration monitor during consecutive time course after pre-dosing triggering. Free drug AL3810 was promptly distributed and eliminated denoting a shortcoming of the non-long-circulating formulation (Fig. 3B). c(RGDyK)-LS/AL3810 was swiftly eliminated and turned undetectable within 30 min incapable of figuring out AUC_{0-48} or MRT_{0-48} by DAS 2.0 (Supporting Information Fig. S8). mn-LS/AL3810 and LS/AL3810 also had greatly shortened blood duration leaving an unmeasurable level at 4 h, decreasing AUC_{0-48} to 50.219 and 53.715 μg/mL·h, respectively. We speculated that the extremely rapid removal in blood stream might be inextricable from the absorption of substantial anti-liposome IgG and IgM stimulated by drug-free counterparts following antibody-induced complement activation and subsequent complement-mediated elimination. c(RGDyK)-LS acted as a potent inducer of IgG titer at 31,813.5 after injecting twice differing from LS and mn-LS ($P < 0.05$), but the equivalent IgM titer as other liposome groups consisting with the former dada on ICR mice (Fig. 3C and D). To separate free antibodies that did not bind onto liposome, we excluded protein-liposome complex from plasma by ultra-centrifugation at 14,000×*g* in 4 °C. The unabsorbed anti-liposome IgG or IgM antibody descent happened to arbitrary liposome group within 30 min after corresponding liposome dosage illustrating that liposome-to-antigen identification and antibody-antigen binding did exist. Most anti-liposome antibody titers dropped and maintained at a certain level, however, free anti-c(RGDyK)-liposome IgM fell to the lowest at 0.5 h and the escalation ensued bringing about a difference of two orders of magnitude from LS/AL3810 and mn-LS/AL3810, which served as a proxy for re-boosting immunization by c(RGDyK)-motif. In the same way, we chose the terminal complements to characterize the potential effect complement activation exerted on. C5b-9 was terminal

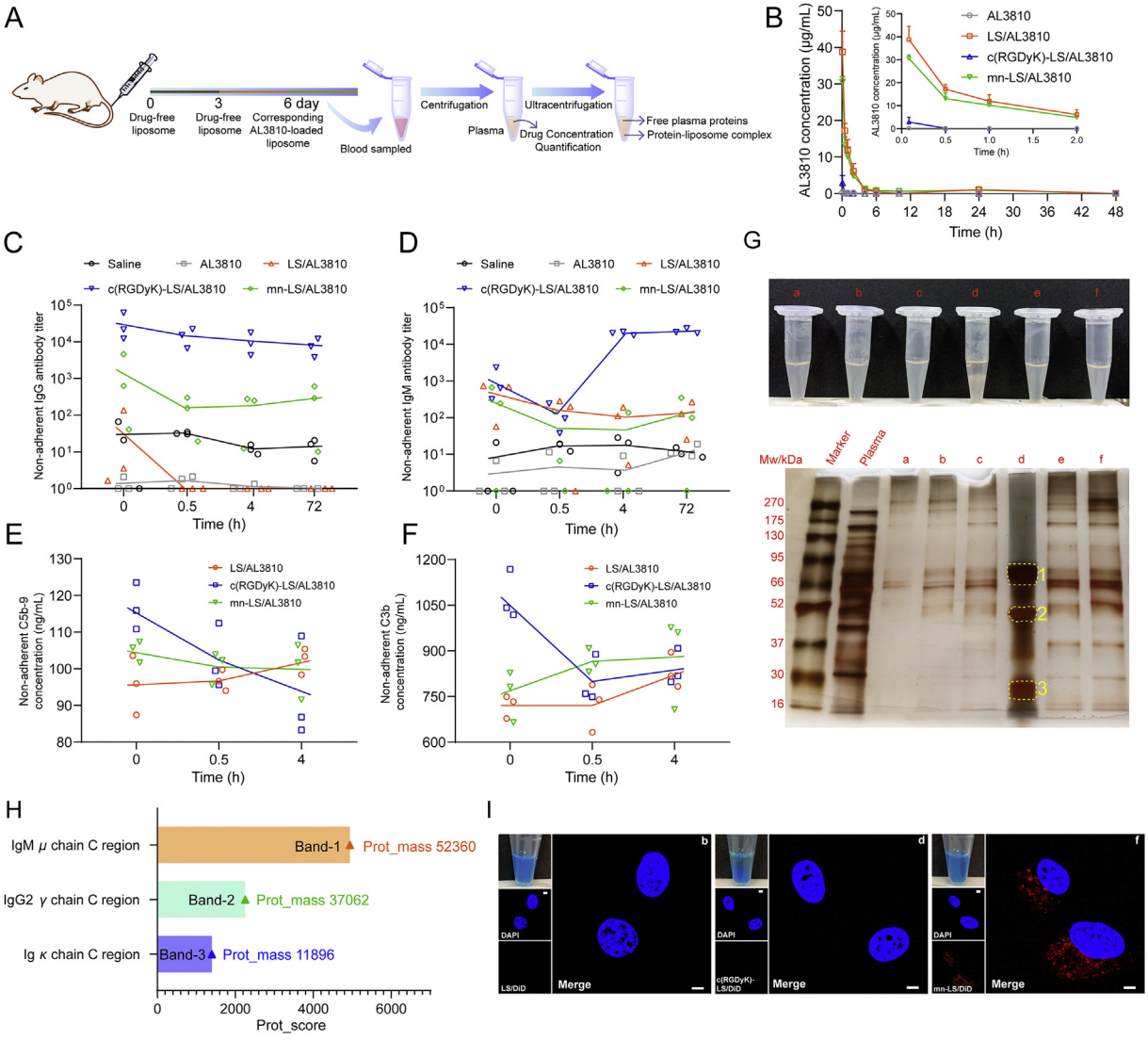

Figure 3 Comprehensive evaluation of multiple dosing. (A) Schematic illustration of drug administration and sample processing. (B) Plasma AL3810 concentration−time diagram upon third sequential administration *via* tail vein (Mean ± SD, $n = 3$). (C) and (D) Time course of non-adherent anti-liposome IgG (C) and IgM (D) antibody titer at 0 h, 0.5 h, 4 h and 72 h post different formulations injection. Antibody titer was obtained *via* ELISA assay (Mean ± SD, $n = 3$). (E) and (F) Concentration changes of non-adherent C5b-9 (E) and C3b (F) in blood along with time of various AL3810-loaded liposomes administration. Concentration was quantified by ELISA kits and reference standards were used for fitting calibration curves (Mean ± SD, $n = 3$). (G) The photograph of resultant mixture from plasma and corresponding liposome at the same volume. The ultra-centrifugal liposome-protein pellet was separated by SDS-PAGE. Group a: LS/AL3810 with equal volume of blank plasma; Group b: LS/AL3810 with equal volume of plasma sampled from LS/AL3810 injected group; Group c: c(RGDyK)-LS/AL3810 with equal volume of blank plasma; Group d: c(RGDyK)-LS/AL3810 with equal volume of plasma sampled from c(RGDyK)-LS/AL3810 injected group; Group e: mn-LS/AL3810 with equal volume of blank plasma; Group f: mn-LS/AL3810 with equal volume of plasma sampled from mn-LS/AL3810 injected group. The loading quantity of group d on SDS-PAGE was one tenth of that of every other group. (H) The protein identification of Band1-3 in group d by Prot_score using nano-LC/MS/MS. (I) The cellular uptake of liposome-plasma mixture by U87 MG cells at 37 °C for 2 h. Identification of group name was the same as above. Intracellular fluorescence was captured by a confocal laser scanning microscope. Scale bar = 5 μm.

complement complex that could attack liposome membrane causing destabilization, and C3b was a complement fragment that could bind the C3b receptor on macrophage giving rise to liposome opsonization, either of which could accelerate liposome clearance. Twice administration of drug-free LS and mn-LS limitedly activated C5b-9 or C3b yet c(RGDyK)-LS unveiled dissimilarity where the unabsorbable C5b-9 concentration was subtly higher ($P < 0.05$ for LS/AL3810) and C3b concentration were far higher ($P < 0.001$ for LS/AL3810 and mn-LS/AL3810, Fig. 3E and F). The inclination of C5b-9 and C3b binding to liposome were exclusively found in c(RGDyK)-LS/AL3810 group as an indication of unabsorbable C5b-9 and C3b diminution while other groups sustained a normal C5b-9 level or slight augmentation of C3b. The foregoing results reflected that the existed anti-liposome antibodies and complements primed by twice administration could bind to the new-coming foreign liposome specifically

engendering rapid clearance, among which c(RGDyK)-motif spurred the most severe immunization commensurate with the shortest blood duration.

To characterize the interaction between liposomes and plasma proteins, all AL3810-loaded liposomes were incubated with the plasma collected from the corresponding liposome treated rats at 0 h in consideration of the maximal antibody amount at that time point. Non-adherent plasma proteins were ultra-centrifuged and the resultant plasma protein pellets were loaded on SDS-PAGE. The fresh plasma from a brand-new rat was directed to the same procedure as control. The absorption of pristine plasma did not alter uniformity and stability of liposome (group a, c and e pointed in Fig. 3G) and not significantly affect nanoparticle size and polydispersity index (Supporting Information Fig. S4D and S4E). LS/AL3810 and mn-LS/AL3810 incubated with the plasma of counterparts stood as they were (groups b and f in Fig. 3G), but c(RGDyK)-LS/AL3810 encountering the plasma of counterpart precipitated quickly with massive sediment observed (group d pointed in Fig. 3G). The colossal sediment imparted by the mixing between c(RGDyk)-liposome and the plasma of c(RGDyk)-liposome-treated rat at a volume ratio of 1:1, was reckoned to be relevant to the torpedoed nanoparticle dynamic stability because of the too thick adherent protein layer[27]. On the other hand, it widely held opinion that insertion of C5b-9 into liposomal bilayer might lead to substantial leakage of the aqueous cargo and liposome flocculation[28]. The precipitation did not happen to other groups pointing up that the antibody and complements c(RGDyk)-liposome incited towered any other group. Besides, no sediment was observed in mn-LS/AL3810 incubated with equal volume of plasma sampled from c(RGDyK)-LS/AL3810 injected rat at 0 h, testifying this intense interaction was with specificity guided by antigen-antibody recognition (Supporting Information Fig. S9). The protein architecture that adhered to liposome surface was quite complicated associating within surface chemistry, as conceptualized as protein corona[29,30]; specific antibody took charge of surface binding once multiple dosage and immunization arousal. The protein corona of mn-LS/AL3810 was more massive than that of LS/AL3810 all along. Nonetheless, mn-LS/AL3810 and LS/AL3810 shared a feature that the protein corona in pristine plasma approximately resembled that in the plasma of the counterpart-injected rat pairwise, but the latter was heavier than the former. The protein corona composition of c(RGDyK)-LS/AL3810 in pristine plasma was similar to that of mn-LS/AL3810, dropping a hint that c(RGDyK)-LS/AL3810 had no unique interplay with natural proteins in plasma. Albeit the loading quantity of group d was solely one tenth of any other group taking into account separation efficiency on SDS-PAGE, the appearance of plentiful protein bands in the lane implied that abundant protein binding occurred to c(RGDyK)-LS/AL3810 *in vivo* when multiple dosing, three of which were main bands around 66, 52 and 30 kDa subsequently subject to nano-LC–MS/MS. The extracted protein after enzymolysis was analyzed by LC−MS/MS and retrieved in data base to identify protein types (Supporting Information Tables S2−4). According to Prot_score, the main protein type in Band-1 was IgM μ chain C region, and one in Band-2 was IgG2 γ chain C region. With a score of 1399, Ig κ chain C region chiefly located in Band-3. Moreover, complement C3, C9 and other complements made up a certain ratio of adherent protein composition (Supporting Information Fig. S10). In a nutshell, immunoglobulin and immunoglobulin-like proteins bound onto c(RGDyK)-LS mainly, C3 and related complements also did vehemently. Since previous results intrigued an appeal to validation of liposome targeting capability after multiple dosages, the DiD-loaded liposome by the same means of incubation was carried out. LS/DiD had no glioma affinity as anticipated (Fig. 3I). The phenomenon that c(RGDyK)-LS/DiD and plasma proteins complex setting off flocculation alike was in responsible for scarce uptake by U87 MG cells and suggestive of the lost targeting ability mainly blunted by the aroused antibodies and complements. The residual targeting ability of mn-LS/DiD through an influence that antibodies and complements might impact on was supported by the captured intracellular fluorescence. In a word, mn-liposome had decent immunocompatibility and did not provoke overfull antibodies and complements that led to malfunction of prolonged circulation and glioma targeting, conversely c(RGDyK)-liposome excited immune reaction out of an allowable range with an odd of hypothermia. Given anti-c(RGDyK)-liposome IgG and IgM antibody, C5b-9 and C3b bound onto new-injected c(RGDyK)-liposome, breakdown of pharmacokinetics and targeting ability was reasonably expounded.

3.8. mn-LS/AL3810 shunned the immune opsonization of macrophage

PEG plays a pivotal role as sheddable liposome coating to avoid being taken up by mononuclear phagocytic system (MPS) and to fulfill prolonged circulation[31]. This PEG effect may be due to avoidance of self-aggregation of liposomes and/or nonspecific dysopsonization phenomenon by which PEG promotes binding of certain proteins that in turn shield the vesicle[32]. But there is a chance that PEGylated nanocarriers could be opsonized by opsonin recognition after peptide ligand decoration. Immune opsonins, particularly complement proteins and antibodies, recognized liposomes as foreign particles and marked them for uptake by macrophages in MPS[33]. Considering the attained result that a great deal of IgG, IgM antibody and complements bound onto corresponding liposomes, skepticism prevailed as to the role that macrophage played on immune opsonization of the targeted liposomes. The opsonized liposome was realized by adding 10% volume of the corresponding immune-triggered plasma. The precipitation could be prevented by lowering 50% plasma composition to 10% (Fig. 4A). Pristine DiD-loaded liposomes were seldom taken up by RAW264.7 cells except for the examined faint red fluorescence of c(RGDyK)-LS/DiD (Supporting Information Fig. S11A). The quantifiable data by flow cytometry gave us better insight that uptake percentage of c(RGDyK)-LS/DiD was 17.3% slightly more than LS/DiD of 1.36% and mn-LS/DiD of 9.97% (Fig. 4B). Phagocytosis by RAW264.7 cells was dominated by particular antibodies or complements that were absent in DMEM culture. The low intake of c(RGDyK)-LS/DiD was reversed by opsonization as delineated as 83.4% fluorescent positive macrophages and 3.1-fold increase of median fluorescent intensity in comparison to pristine counterpart (Fig. 4A−C). The interrogation into cellular uptake of the opsonized liposomes untangled the opsonic effect of macrophage undoubtedly. Insufficient antibodies and complements in plasma constituent that mn-motif elicited did not assisted mn-LS/DiD to be recognized by macrophages as the invariable uptake percentage and median fluorescent intensity acquired. Antibody-liposome complex could weaken the complement system with substantial downstream complement proteins energized[34], proved by authenticated complement-opsonized liposomes formed by binding with antibodies and complements in above investigation (Fig. 3). Manifold signaling molecule

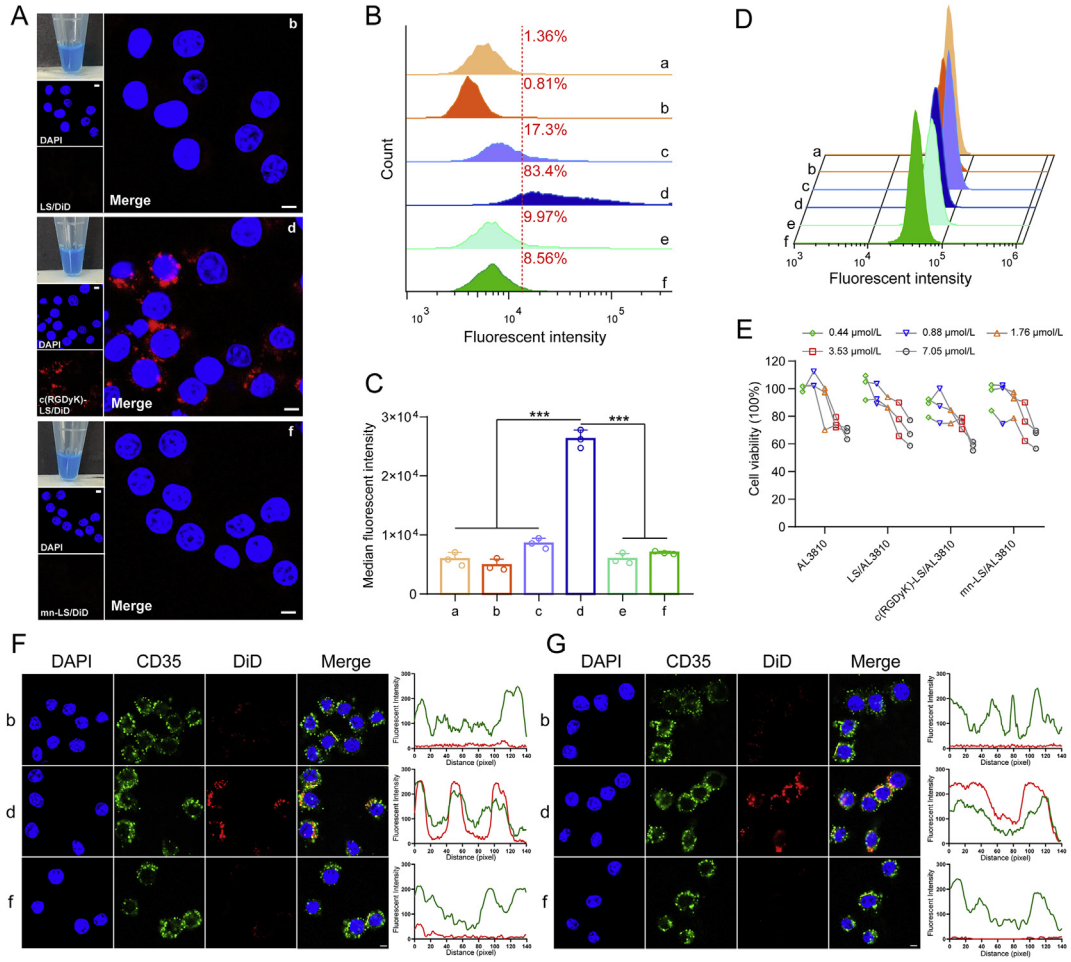

Figure 4 Reciprocity of immune opsonized liposomes and macrophage. (A)−(C) The cellular uptake of immune opsonized DiD-loaded liposome by RAW264.7 cells at 37 °C for 4 h. Intracellular fluorescence was captured by a confocal laser scanning microscope (A). Scale bar = 5 μm. Uptake percentage (B) and median fluorescent intensity (C) was gauged by flow cytometry. Group a: pristine LS/AL3810; Group b: LS/AL3810 with 10% volume of plasma sampled from LS/AL3810 injected group; Group c: pristine c(RGDyK)-LS/AL3810; Group d: c(RGDyK)-LS/AL3810 with 10% volume of plasma sampled from c(RGDyK)-LS/AL3810 injected group; Group e: pristine mn-LS/AL3810; Group f: mn-LS/AL3810 with 10% volume of plasma sampled from mn-LS/AL3810 injected group (Mean ± SD, $n = 3$, $^{***}P < 0.001$). (D) The cellular uptake of immune opsonized DiD-loaded liposome by hepatocytes (AML 12 cells) at 37 °C for 4 h. Identification of group name was the same as above. (E) Cytotoxicity of the AL3810-loaded liposomes on RAW264.7 cells after 48 h exposure. Cell viability was measured by MTT assay. (F)−(G) Colocalization of CD35 and DiD-labeled liposome in RAW264.7 cells after incubation with opsonized DiD-loaded liposome at 37 °C for 1 h (F) and 4 h (G). The corresponding fluorescence calculated by pixel intensity using Image J software were presented, the red line stood for DiD fluorescence, and the green line stood for anti-CD35 antibody fluorescence. Intracellular fluorescence was captured by a confocal laser scanning microscope. Identification of group name was the same as above. Scale bar = 5 μm.

interacted mutually when immune opsonization, for instance, the adherent C3b of opsonized liposomes could anchor C3b receptor on macrophage, which was responsible for enhanced macrophage uptake[35]. As shown in Fig. 4F and G, CD35 (C3b receptor) was a membrane-bound glycoprotein ubiquitously found on macrophages visualized by anti-CD35 antibody[36]. The engulfed c(RGDyK)-liposome was overlapped with CD35 precisely with the help of plasma constituent after 1-h incubation, and c(RGDyK)-liposome entered into cytoplasmic fervently after 4-h incubation as red fluorescence range sort of surpassed green fluorescence range. In spite of CD35 popularity on RAW264.7 cells membrane, mn-liposome uptake was lightly aided by plasma incubation in terms of inadequate C3b activated in plasma. To decipher whether it was ascribed to lipoprotein-driven opsonization, we managed the same assay on hepatocyte for its abundant scavenger receptor, apo-lipoprotein and lipoprotein receptors on the surface[37,38]. Withal, it come out no discernible fluorescence increment through opsonic plasma incubation, which was educed that c(RGDyK)-liposome opsonization was immunogenic and complement-driven (Fig. 4D and Supporting Information Fig. S11B and S11C). Next, we tackled the reason why immunogenicity issue of well-recognized c(RGDyK)-liposome applied to chemotherapeutic agents was unreported before. We chose doxorubicin as a model drug for chemotherapeutic agents and AL3810 for molecular targeting agents, and loaded into various liposomes alike[39]. 7.05 μmol/L AL3810 dosage revealed mild cytotoxicity against macrophages as over 50% viability after 48 h incubation (Fig. 4E). On the contrary, 1.08 μmol/L free drug DOX resulted in 90% macrophage death after 48 h, and cytotoxic potency of DOX-loaded liposome against macrophages was 1.5−3.0 times that of AL3810-loaded liposomes (Supporting Information Fig. S12). No obvious immunogenicity

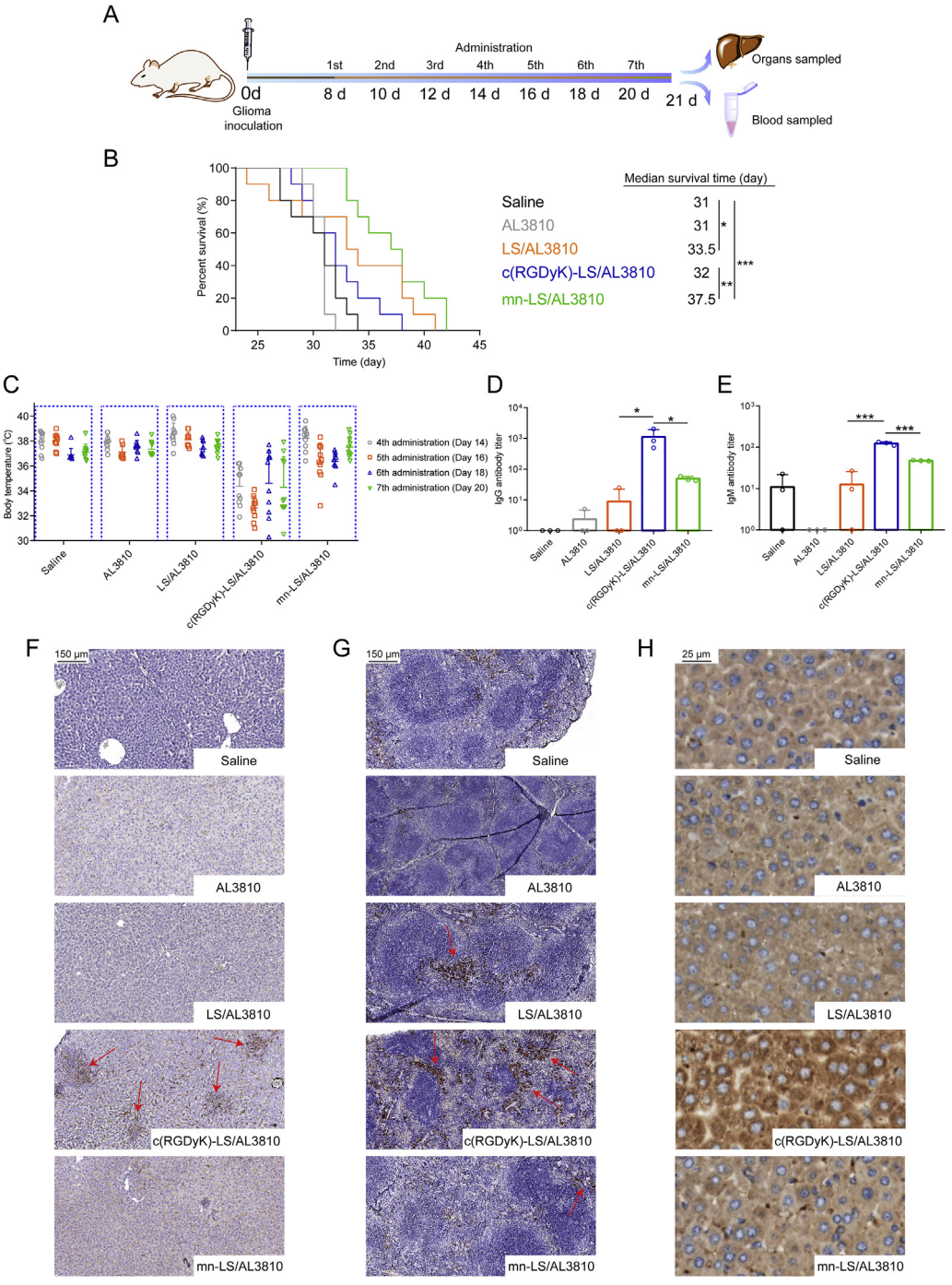

Figure 5 *In vivo* anti-glioma effect and immune response of the targeted AL3810-loaded liposomes on nude mice. (A) Schematic illustration of glioma inoculation, drug administration and sample processing. (B) Kaplan−Meier survival curves of nude mice bearing U87 MG orthotopic xenograft (Mean ± SD, $n = 10$, $^{*}P < 0.05$, $^{**}P < 0.01$, $^{***}P < 0.001$). (C) The body temperature record of U87 MG orthotopic xenograft bearing nude mice at 0.5 h after injecting different formulations of the equal AL3810 doses. Data was collected from forehead thermometer (Mean ± SD, $n = 10$). (D) and (E) Titer determination of anti-liposome IgG (D) and IgM (E) antibody by ELISA assay in blood of U87 MG orthotopic xenograft bearing nude mice. Corresponding liposome was used as antigen (Mean ± SD, $n = 3$, $^{*}P < 0.05$, $^{***}P < 0.001$). (F) and (G) Antibody-liposome complex deposition in liver (F) and spleen (G) of U87 MG orthotopic xenograft bearing nude mice. Red arrows pointed at obvious deposition. (H) Complement C3 deposition that was brown in liver sections of U87 MG orthotopic xenograft bearing nude mice.

was inspected when c(RGDyK)-liposome was employed to deliver chemotherapeutic agents accounting for immunosuppressive effect with indiscriminative cytotoxicity towards immune system including macrophages[40]. Molecular targeting agent AL3810 anchored VEGFR and FGFR having negligible immunosuppression so that AL3810-loaded c(RGDyK)-liposome triggered immune reaction dramatically and conduced detectable hypothermia. The superior alternative mn decorating liposome exhibited the

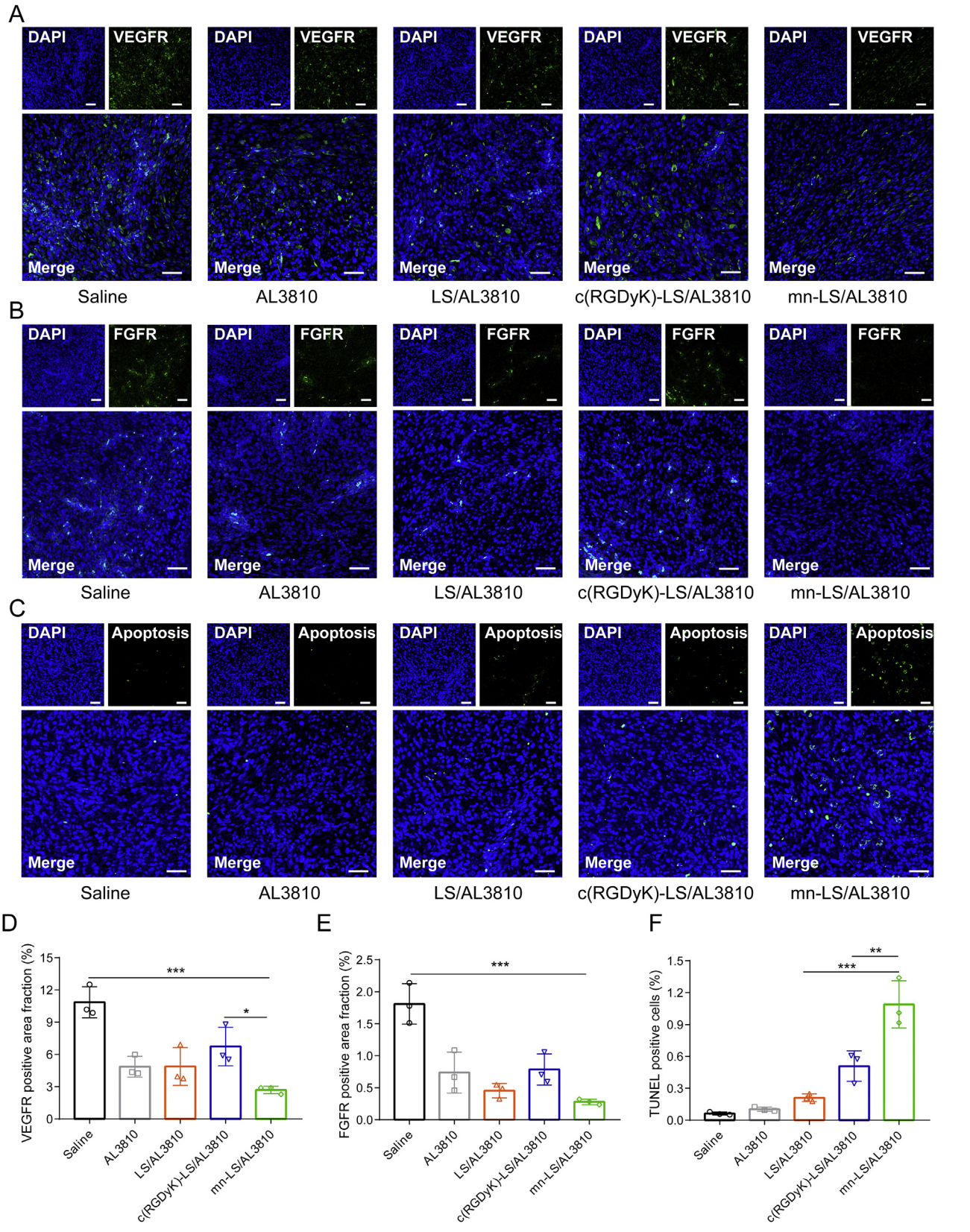

Figure 6 *In vivo* regulation of VEGFR and FGFR in glioma that AL3810 liposomal formulations imposed on. (A)−(F) VEGFR immunofluorescence staining (A) and quantification of VEGFR positive cells (D); FGFR immunofluorescence staining (B) and quantification of FGFR positive cells (E); TUNEL immunofluorescence staining (C) and quantification of cell apoptosis (F) of the glioma tissues of the mice bearing U87 MG orthotopic xenograft the next day after various treatments (Day 21). Scale bar = 50 μm. Data are Mean ± SD, $n = 3$; $^{**}P < 0.01$, $^{***}P < 0.001$.

attenuated immunogenicity, more importantly, and shunned the immune opsonization.

3.9. *mn-LS/AL3810 exhibited decent immunocompatibility and therapeutic prowess on glioma orthotopic xenograft*

In the wake of nanotechnology popularity, ligand is grafted onto the larger scaffolds to materialize targeting tumor actively. However, the jury is still out on immunogenicity matter that peptide-grafted nanocarriers may be identified as heterologous protein and treated as antigen. Especially when loading low-toxic molecular targeting agent, immunocompatibility safety become a momentous concern. Initially the U87 MG orthotopic xenograft was constructed as described before, the modeled nude mice were injected with different AL3810 formulations *via* tail vein from Day 8 at a frequency of every other day. The blood and organs were sampled for various analysis the next day after accomplishment of treatment course (Fig. 5A). In the course of injection, the bodyweight of drug-treated groups was subtly lighter than saline group but still heavier than the initial value, explicitly demonstrating the weak systemic toxicity (Supporting Information Fig. S13). Ending up with drug administration (day 20), the bodyweight precipitously declined in pace with pathological progression. According to HE sections of organs, all AL3810 formulations did not visibly impair organs apart from minute hepatocytes cytoplasmic loosening in liver and multinucleated giant cells in spleen, which c(RGDyK)-LS/AL3810-treated group suffered the most (Supporting Information Fig. S14A). As shown in Fig. 5B, mn-LS/AL3810 achieved the best treatment outcome by prolonging the median survival time to 37.5 days outgrowing the other groups treated with saline (31 days), free AL3810 (31 days), LS/AL3810 (33.5 days) and c(RGDyK)-LS/AL3810 (32 days, $P < 0.01$). Limited by immune opsonization and body damage by hypothermia, c(RGDyK)-LS/AL3810 did a worse therapy outcome than LS/AL3810. Accordingly, mn-LS/AL3810 inhibited more glioma angiogenesis outstripping other liposomes and free drug (Supporting Information Fig. S14B and S14C). What is more, mn-LS/AL3810 posed a powerful hurdle for VEGFR and FGFR expression, which was superior to c(RGDyK)-LS/AL3810 and LS/AL3810, and offered more inducement of apoptosis ($P < 0.01$ compared with c(RGDyK)-LS/AL3810, Fig. 6). Pharmacological mechanism reciprocally explicated the section analysis and treatment result.

BALB/c athymic nude mice with T-cell-mediated immunity deficiency could accept major histocompatibility complex mismatched xenografts[41]. Howbeit innate immunity and humoral immunity function well, and B cells and natural killer cells, macrophages and dendritic cells stay active[42], appropriately reflective of antibody production and humoral immune response. As discussed previously, the record of belly temperature at 30 min post injection might be indicative of immune response (Fig. 5C). The fourth c(RGDyK)-LS/AL3810 started to render a large cohort of mice hypothermia (below 34 °C), the fifth was the most severe and the sixth administration had toughened mice into being tolerant. Two of ten mice treated with the fourth mn-LS/AL3810 started hypothermia, a majority kept body temperature around 36 °C when the fifth and sixth injection, and all returned to normal when the last injection. Other groups did not generate palpable hypothermia. In mice, immediate hypothermia is a typical characteristic of systemic anaphylaxis and has been regarded as a barometer of the onset of anaphylaxis in many studies[43,44]. And there is a chance that the complement activation triggered by immune complex lead to anaphylaxis *via* the release of anaphylatoxins and other subsequent reactions[45]. Taken together, multiple sequential injection of peptide-tethered AL3810-loaded liposomes did bolster immune reaction on nude mice. There was a regular pattern that hypothermia distinctly arose from the fourth, bottomed at the fifth and relapsed from the sixth injection, among which the probability and severity that mn-LS/AL3810 led to were fairly lower than that of c(RGDyK)-LS/AL3810. The anti-liposome IgG titer also told that c(RGDyK)-LS/AL3810 sensitized immune mechanism profoundly in the course of treatment with a conspicuous discrepancy ($P < 0.05$ compared with LS/AL3810 and mn-LS/AL3810), as was IgM titer ($P < 0.001$ compared with LS/AL3810 and mn-LS/AL3810, Fig. 5D and E). Furthermore, we found appreciable antibody-antigen complex deposition in liver and spleen of c(RGDyK)-liposome-injected group. The location the red arrow pointed at was full of antibody-c(RGDyK)-liposome complex deposition, suggesting that c(RGDyK)-liposome could trigger immune response in liver (Fig. 5F). The observed antibody-c(RGDyK)-liposome complex mostly located in the marginal zone of spleen where a ring of macrophages resided[46], which was also attributed to enhanced immune opsonization in spleen (Fig. 5G). Complement activation mainly took place in liver[47]. As for C3 deposition in liver, mn-LS/AL3810 apparently fomented less complement activation in liver than c(RGDyK)-LS/AL3810 (Fig. 5H and Supporting Information Fig. S15). The single dose could not mirror the immunogenicity of liposomes; when a whole regimen course with multi-dose, antibodies elicited by peptide-modified liposome took part in blood elimination, liver and spleen sequestration, reinventing targeting efficiency and therapeutic outcome. The anti-glioma efficiency of AL3810 liposomal formulations could be compromised by immune reaction, which caused accelerated elimination and even certain off-target effects. With the notion that c(RGDyK)-liposome encapsulating low-toxicity drugs possessed considerable immunogenicity, as a consequence, mn-targeted liposome loading AL3810 was engineered to reconcile attenuated immunogenicity and glioma-targeted curative criterion.

4. Conclusions

AL3810 is a dual inhibitor of the ATP pocket on intracellular region of VEGF and FGF receptors in a variety of tumor treatments, but deficient in glioma therapy as poor addressability of BBTB recognition and penetration. We formulated AL3810-loaded liposome with uniformity and stability at high entrapment efficiency by using ammonium sulfate gradient loading method. AL3810-loaded liposome modified by a well-accepted $\alpha v\beta 3$ ligand c(RGDyK) was prone to render hypothermia and be undermined by the unwanted inclination of immune opsonization initialed by binding existed anti-c(RGDyK)-liposome IgG and IgM, C3 and C5b-9. We put forth a novel $\alpha v\beta 3$-targeted peptide mn with decent glioma-targeted capability corroborated. More importantly, mn-liposome abated the opsonic effect as lower anti-mn-liposome IgG and IgM antibody titer, less antibody binding, less complements activation and subsequently less phagocytosis by macrophages. Consequently AL3810-loaded mn-liposome efficiently down-regulated EGFR protein, induced apoptosis of glioma cells, restrained EGF and FGF-driven glioma angiogenesis *in vitro*, and successfully conveyed AL3810 into glioma, and also preserved the extended circulation longevity after multiple dosage as envisioned. The above multifaceted superiorities extended

glioma treatment benefit. Now that different peptide modifications onto liposomes make a big difference on immunogenicity that exerted a pivotal impact on bio-fate, immune-compatibility evaluation of nanomedicine turns out requisite. This research introduces mn-based nanoscopic liposome for AL3810 delivery with attenuated immunogenicity that outmaneuvered immune opsonization, which appears to have clinical translatability for safe and effective glioma-targeted liposomal drug formulations.

Acknowledgments

This work was supported by the National Natural Science Foundation of China (Nos. 81773657, and 81690263), Innovation Program of Shanghai Municipal Education Commission (2017-01-07-00-07E00052, China) and National Basic Research Program of China (973 Program, No. 2013CB932500, China).

Author contributions

Jinyang Li and Weiyue Lu designed the research. Jinyang Li, Jiasheng Lu and Haiyan Guo carried out the experiments. Jianfen Zhou, Songli Wang, Kuan Jiang, Zhilan Chai and Shengyu Yao participated part of the experiments. Xiaoyi Wang, Linwei Lu and Cao Xie performed data analysis. Yi Chen provided experimental drugs. Jinyang Li drafted the manuscript. Weiyue Lu revised the manuscript and supervised the project. All of the authors have read and approved the final manuscript.

Conflicts of interest

The authors have no conflicts of interest to declare.

Appendix A. Supporting information

Supporting data to this article can be found online at https://doi.org/10.1016/j.apsb.2020.07.024.

References

1. Viallard C, Larrivee B. Tumor angiogenesis and vascular normalization: alternative therapeutic targets. *Angiogenesis* 2017;**20**:409−26.
2. Carmeliet P, Jain RK. Principles and mechanisms of vessel normalization for cancer and other angiogenic diseases. *Nat Rev Drug Discov* 2011;**10**:417−27.
3. Carmeliet P, Jain RK. Molecular mechanisms and clinical applications of angiogenesis. *Nature* 2011;**473**:298−307.
4. Huang H, Held-Feindt J, Buhl R, Mehdorn HM, Mentlein R. Expression of VEGF and its receptors in different brain tumors. *Neurol Res* 2005;**27**:371−7.
5. Mentlein R, Forstreuter F, Mehdorn HM, Held-Feindt J. Functional significance of vascular endothelial growth factor receptor expression on human glioma cells. *J Neuro Oncol* 2004;**67**:9−18.
6. Smith SJ, Ward JH, Tan C, Grundy RG, Rahman R. Endothelial-like malignant glioma cells in dynamic three dimensional culture identifies a role for VEGF and FGFR in a tumor-derived angiogenic response. *Oncotarget* 2015;**6**:22191−205.
7. Bello E, Colella G, Scarlato V, Oliva P, Berndt A, Valbusa G, et al. E-3810 is a potent dual inhibitor of VEGFR and FGFR that exerts antitumor activity in multiple preclinical models. *Cancer Res* 2011;**71**:1396−405.
8. Zhou Y, Chen Y, Tong L, Xie H, Wen W, Zhang J, et al. AL3810, a multi-tyrosine kinase inhibitor, exhibits potent anti-angiogenic and anti-tumour activity *via* targeting VEGFR, FGFR and PDGFR. *J Cell Mol Med* 2012;**16**:2321−30.
9. Roberts WG, Delaat J, Nagane M, Huang S, Cavenee WK, Palade GE. Host microvasculature influence on tumor vascular morphology and endothelial gene expression. *Am J Pathol* 1998;**153**:1239−48.
10. Vick NA, Bigner DD. Microvascular abnormalities in virally-induced canine brain tumors: structural bases for altered blood−brain barrier function. *J Neurol Sci* 1972;**17**:29−39.
11. Zhan C, Gu B, Xie C, Li J, Liu Y, Lu W. Cyclic RGD conjugated poly(ethylene glycol)-*co*-poly(lactic acid) micelle enhances paclitaxel anti-glioblastoma effect. *J Control Release* 2010;**143**:136−42.
12. Zhao X, Chen R, Liu M, Feng J, Chen J, Hu K. Remodeling the blood−brain barrier microenvironment by natural products for brain tumor therapy. *Acta Pharm Sin B* 2017;**7**:541−53.
13. Ye C, Pan B, Xu H, Zhao Z, Shen J, Lu J, et al. Co-delivery of GOLPH3 siRNA and gefitinib by cationic lipid−PLGA nanoparticles improves EGFR-targeted therapy for glioma. *J Mol Med (Berl)* 2019;**97**:1575−88.
14. Kwatra MM. A rational approach to target the epidermal growth factor receptor in glioblastoma. *Curr Cancer Drug Targets* 2017;**17**:290−6.
15. Wohlfart S, Gelperina S, Kreuter J. Transport of drugs across the blood−brain barrier by nanoparticles. *J Control Release* 2012;**161**:264−73.
16. Wicki A, Witzigmann D, Balasubramanian V, Huwyler J. Nanomedicine in cancer therapy: challenges, opportunities, and clinical applications. *J Control Release* 2015;**200**:138−57.
17. Su H, Wang Y, Liu S, Wang Y, Liu Q, Liu G, et al. Emerging transporter-targeted nanoparticulate drug delivery systems. *Acta Pharm Sin B* 2019;**9**:49−58.
18. Desgrosellier JS, Cheresh DA. Integrins in cancer: biological implications and therapeutic opportunities. *Nat Rev Canc* 2010;**10**:9−22.
19. Wang X, Meng N, Wang S, Zhang Y, Lu L, Wang R, et al. Non-immunogenic, low-toxicity and effective glioma targeting MTI-31 liposomes. *J Control Release* 2019;**316**:381−92.
20. Wang X, Wang H, Jiang K, Zhang Y, Zhan C, Ying M, et al. Liposomes with cyclic RGD peptide motif triggers acute immune response in mice. *J Control Release* 2019;**293**:201−14.
21. Li J, Chai Z, Lu J, Xie C, Ran D, Wang S, et al. $\alpha v\beta 3$-targeted liposomal drug delivery system with attenuated immunogenicity enabled by linear pentapeptide for glioma therapy. *J Control Release* 2020;**322**:542−54.
22. Lei Y, Wang J, Xie C, Wagner E, Lu W, Li Y, et al. Glutathione-sensitive RGD-poly(ethylene glycol)-SS-polyethylenimine for intracranial glioblastoma targeted gene delivery. *J Gene Med* 2013;**15**:291−305.
23. Guan J, Shen Q, Zhang Z, Jiang Z, Yang Y, Lou M, et al. Enhanced immunocompatibility of ligand-targeted liposomes by attenuating natural IgM absorption. *Nat Commun* 2018;**9**:2982.
24. Wei X, Gao J, Zhan C, Xie C, Chai Z, Ran D, et al. Liposome-based glioma targeted drug delivery enabled by stable peptide ligands. *J Control Release* 2015;**218**:13−21.
25. Xie Q, Chen H, Ai J, Gao YL, Geng MY, Ding J, et al. Evaluation of *in vitro* and *in vivo* activity of a multityrosine kinase inhibitor, AL3810, against human thyroid cancer. *Acta Pharmacol Sin* 2017;**38**:1533−42.
26. Balbino B, Sibilano R, Starkl P, Marichal T, Gaudenzio N, Karasuyama H, et al. Pathways of immediate hypothermia and leukocyte infiltration in an adjuvant-free mouse model of anaphylaxis. *J Allergy Clin Immunol* 2017;**139**:584−96. e10.
27. Aguilar-Castillo BA, Santos JL, Luo H, Aguirre-Chagala YE, Palacios-Hernández T, Herrera-Alonso M. Nanoparticle stability in biologically relevant media: Influence of polymer architecture. *Soft Matter* 2015;**11**:7296−307.

28. Moghimi SM, Hamad I. Liposome-mediated triggering of complement cascade. *J Liposome Res* 2008;**18**:195−209.
29. Bigdeli A, Palchetti S, Pozzi D, Hormozi-Nezhad MR, Baldelli Bombelli F, Caracciolo G, et al. Exploring cellular interactions of liposomes using protein corona fingerprints and physicochemical properties. *ACS Nano* 2016;**10**:3723−37.
30. Bertrand N, Grenier P, Mahmoudi M, Lima EM, Appel EA, Dormont F, et al. Mechanistic understanding of *in vivo* protein corona formation on polymeric nanoparticles and impact on pharmacokinetics. *Nat Commun* 2017;**8**:777.
31. Dadashzadeh S, Mirahmadi N, Babaei MH, Vali AM. Peritoneal retention of liposomes: effects of lipid composition, PEG coating and liposome charge. *J Control Release* 2010;**148**:177−86.
32. Moghimi SM, Szebeni J. Stealth liposomes and long circulating nanoparticles: critical issues in pharmacokinetics, opsonization and protein-binding properties. *Prog Lipid Res* 2003;**42**:463−78.
33. Yan X, Scherphof GL, Kamps JA. Liposome opsonization. *J Liposome Res* 2005;**15**:109−39.
34. Gaboriaud C, Thielens NM, Gregory LA, Rossi V, Fontecilla-Camps JC, Arlaud GJ. Structure and activation of the C1 complex of complement: unraveling the puzzle. *Trends Immunol* 2004;**25**:368−73.
35. Scherphof GL, Kamps JAAM. Receptor *versus* non-receptor mediated clearance of liposomes. *Adv Drug Deliv Rev* 1998;**32**:81−97.
36. Liu D, Niu ZX. The structure, genetic polymorphisms, expression and biological functions of complement receptor type 1 (CR1/CD35). *Immunopharmacol Immunotoxicol* 2009;**31**:524−35.
37. Yan X, Poelstra K, Scherphof GL, Kamps JAAM. A role for scavenger receptor B-I in selective transfer of rhodamine-PE from liposomes to cells. *Biochem Biophys Res Commun* 2004;**325**:908−14.
38. Scherphof GL, Kamps JAAM. The role of hepatocytes in the clearance of liposomes from the blood circulation. *Prog Lipid Res* 2001;**40**:149−66.
39. Yan Z, Wang F, Wen Z, Zhan C, Feng L, Liu Y, et al. LyP-1-conjugated PEGylated liposomes: A carrier system for targeted therapy of lymphatic metastatic tumor. *J Control Release* 2012;**157**:118−25.
40. Dobrovolskaia MA, Germolec DR, Weaver JL. Evaluation of nanoparticle immunotoxicity. *Nat Nanotechnol* 2009;**4**:411−4.
41. Szadvari I, Krizanova O, Babula P. Athymic nude mice as an experimental model for cancer treatment. *Physiol Res* 2016;**65**:S441−53.
42. Piguet PF. Change in the humoral response of athymic nude mice with ageing. *Scand J Immunol* 1980;**12**:233−8.
43. Tsujimura Y, Obata K, Mukai K, Shindou H, Yoshida M, Nishikado H, et al. Basophils play a pivotal role in immunoglobulin-G-mediated but not immunoglobulin-E-mediated systemic anaphylaxis. *Immunity* 2008;**28**:581−9.
44. Jiao D, Liu Y, Lu X, Liu B, Pan Q, Liu Y, et al. Macrophages are the dominant effector cells responsible for IgG-mediated passive systemic anaphylaxis challenged by natural protein antigen in BALB/c and C57BL/6 mice. *Cell Immunol* 2014;**289**:97−105.
45. Munoz-Cano R, Picado C, Valero A, Bartra J. Mechanisms of anaphylaxis beyond IgE. *J Investig Allergol Clin Immunol* 2016;**26**:73−82.
46. Mebius RE, Kraal G. Structure and function of the spleen. *Nat Rev Immunol* 2005;**5**:606−16.
47. Gao B, Jeong WI, Tian Z. Liver: an organ with predominant innate immunity. *Hepatology* 2008;**47**:729−36.